Microfluidic mixer designed for performing single-molecule kinetics with confocal detection on timescales from milliseconds to minutes

Bengt Wunderlich[1], Daniel Nettels[1], Stephan Benke[1], Jennifer Clark[1], Sascha Weidner[1], Hagen Hofmann[1], Shawn H Pfeil[2,3] & Benjamin Schuler[1]

[1]Department of Biochemistry, University of Zurich, Zurich, Switzerland. [2]Department of Physics, University of California, Santa Barbara, California, USA. [3]Present address: Department of Physics, West Chester University of Pennsylvania, West Chester, Pennsylvania, USA. Correspondence should be addressed to B.S. (schuler@bioc.uzh.ch) or D.N. (nettels@bioc.uzh.ch).

Published online 11 July 2013; doi:10.1038/nprot.2013.082

Microfluidic mixing in combination with single-molecule spectroscopy allows the investigation of complex biomolecular processes under non-equilibrium conditions. Here we present a protocol for building, installing and operating microfluidic mixing devices optimized for this purpose. The mixer is fabricated by replica molding with polydimethylsiloxane (PDMS), which allows the production of large numbers of devices at a low cost using a single microfabricated silicon mold. The design is based on hydrodynamic focusing combined with diffusive mixing and allows single-molecule kinetics to be recorded over five orders of magnitude in time, from 1 ms to ~100 s. Owing to microfabricated particle filters incorporated in the inlet channels, the devices provide stable flow for many hours to days without channel blockage, which allows reliable collection of high-quality data. Modular design enables rapid exchange of samples and mixing devices, which are mounted in a specifically designed holder for use with a confocal microscopy detection system. Integrated Peltier elements provide temperature control from 4 to 37 °C. The protocol includes the fabrication of a silicon master, production of the microfluidic devices, instrumentation setup and data acquisition. Once a silicon master is available, devices can be produced and experiments started within ~1 d of preparation. We demonstrate the performance of the system with single-molecule Förster resonance energy transfer (FRET) measurements of kinetics of protein folding and conformational changes. The dead time of 1 ms, as predicted from finite element calculations, was confirmed by the measurements.

INTRODUCTION

Single-molecule spectroscopy has become an integral part of biophysical research, and a wide range of biological questions are now addressed with this type of method[1], including the mechanisms of molecular machines[2–4], protein-nucleic acid interactions[5,6], enzymatic reactions[7,8] and protein or RNA folding[9,10]. One benefit of single-molecule experiments is that they provide access to information on dynamics with equilibrium measurements, e.g., via correlation functions[11–15], through the analysis of broadening and exchange between subpopulations in FRET efficiency histograms[16–19] or directly from fluorescence trajectories of immobilized molecules[15,18,20–25]. However, in many cases, it remains essential to probe non-equilibrium dynamics, especially if the reaction of interest is essentially irreversible during the observation time accessible at equilibrium or if states or conformations need to be investigated whose populations are too small to be detectable at equilibrium. Examples are association reactions of very stable biomolecular complexes[26,27] or the transient population of unfolded states in protein-folding reactions under conditions that strongly favor the folded state[12,26,28–30]. Obtaining these kinetics requires perturbation methods, such as rapid changes in solution conditions or temperature. These are well-established techniques (e.g., stopped-flow mixing or temperature jump), but only for measurements of ensemble-averaged properties. To make use of the full potential of single-molecule detection for resolving structural heterogeneity and addressing complex kinetic mechanisms, perturbation methods need to be adapted to single-molecule spectroscopy.

Microfluidic mixing[31,32] has been found to be particularly well suited for use with single-molecule detection because it allows direct optical interfacing of devices with the high-numerical-aperture, short-working-distance objective lenses commonly used in single-molecule instruments[28]. The absence of turbulence in microfluidic devices, owing to the small feature sizes and the low flow velocities (i.e., very small Reynolds numbers)[31], results in laminar flow, which can be calculated for complex geometries with the help of finite-element methods[33]. By taking into account the diffusion coefficients of the solutes, the properties of the mixing system can be predicted with high accuracy (**Fig. 1**), which enables stringent device design. Finally, very small sample volumes are required (tens of microliters), which allows kinetic experiments to be performed even in cases where large-scale sample preparation is not feasible.

Since the first application of microfluidic mixing to single-molecule experiments[28], this methodology has been used in a variety of implementations, including microfabrication in silicon[28] and fused silica[34,35], soft lithography[8,12,26,27,29,36–40] and microcapillaries[30], but only recently has the technique matured to a level that allows routine use for a wide range of questions. A key step was the use of replica molding with PDMS[41], which enables the reliable production of large numbers of devices at a low cost based on a single microfabricated silicon mold. Bonding to microscope cover slides allows convenient interfacing of the mixers with a suitable detection system. The device whose fabrication and use is demonstrated here is an improved design based on that of Pfeil *et al.*[38], and it uses hydrodynamic focusing combined with diffusive mixing[32] to achieve millisecond dead times.

Overview of the procedure

The protocol includes step-by-step instructions for the following: fabrication of the silicon master from a photolithographic mask

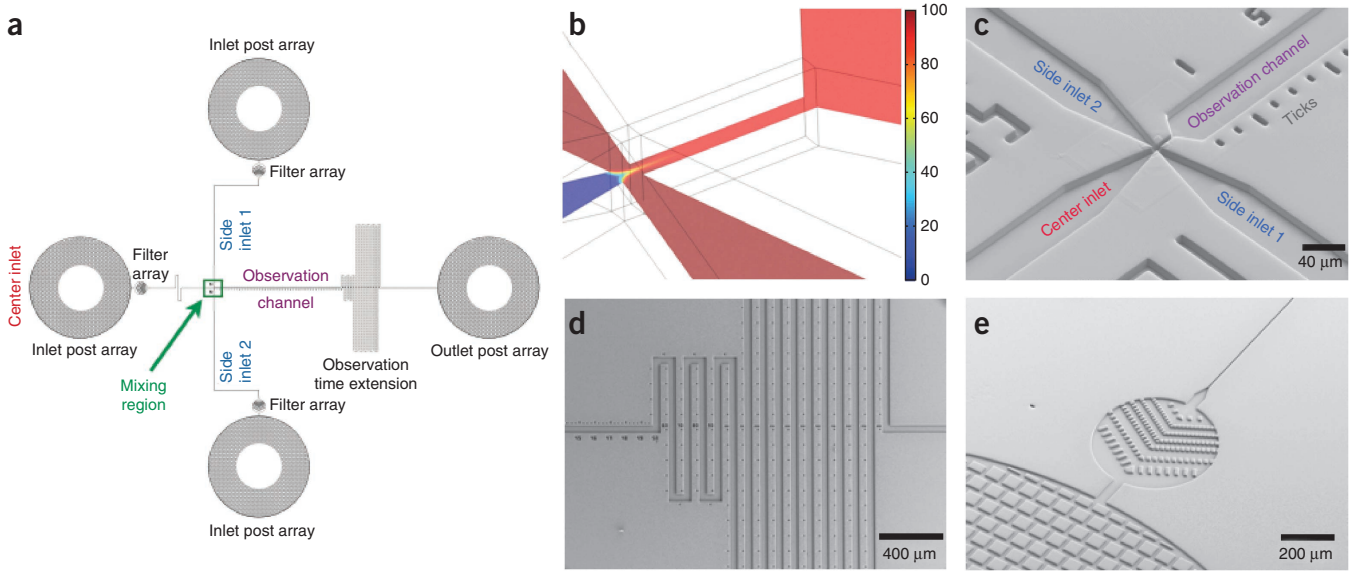

Figure 1 | Microfluidic mixing device allowing observation on timescales from milliseconds to minutes. (**a**) Layout of the microfluidic mixing device. Pressurized air drives the liquids through the center and the two side inlets towards the mixing region. Post arrays prevent collapsing of the PDMS in the large inlets[38], and holes are punched into these arrays to allow the solutions to be supplied. Filter post arrays prevent blockage of the device by dust or other particles. Sample molecules leaving the mixing region pass through the wide observation channel before reaching the outlet post array. The observation time extension (serpentine channel) allows observation times up to minutes. (**b**) Example of a concentration profile from 3D finite-element calculations of the mixing process used for optimization of the chip design. Mixing of buffer (center inlet) with denaturant (side inlets) at a 1:10 ratio is shown. The relative concentration of denaturant is color-coded (see color scale from 0 to 100% denaturant). (**c**) Electron micrograph of the mixing region. Ticks along the observation channel indicate the distance to the center of the mixing region. (Small ticks are separated by 25 µm.) (**d**) Observation time extension. (**e**) Filter post array with six rows of decreasing post separation (20,10,5,4,2,2 µm) connected to the inlet post array to prevent small particles (e.g., dust) from entering the channels and blocking the mixing region. The depth of all features is 10 µm.

(**Supplementary Data 1**), casting of the microfluidic devices in PDMS, their subsequent bonding to a cover slide, and mounting and operating the devices in a specifically designed holder installed on the inverted microscope of a confocal single-molecule instrument.

We provide detailed technical drawings of the device holder, which includes pressure connections required to drive the flow, sample loading and temperature control. We demonstrate the performance of the mixing device with examples of kinetic single-molecule FRET measurements. This design is used routinely in our laboratory to study a variety of questions for which kinetically resolved single-molecule FRET experiments are required, especially in the context of protein folding and protein-protein interactions[12,26,29,42].

Experimental design

Device design. Figure 1 summarizes the layout and key elements of the device. Three inlet channels allow the solutions to be combined in the mixing region (**Fig. 1a**), in which a narrow mixing channel of 2.5-µm width ensures rapid exchange of the components by diffusion perpendicular to the direction of flow (**Fig. 1b,c**). In the following observation channel, the flow velocity is reduced to ~1 µm ms^{-1}, which allows sufficient residence times for the fluorescence of molecules to be detected while they pass through the confocal observation volume. By positioning the confocal volume at different points along the observation channel, different times after mixing can be monitored, and the kinetics of the process can be obtained from the combined analysis of these measurements. The earliest time accessible in the current device is 1 ms (see Anticipated results). (Dead times down to about 0.2 ms have recently been reported[27,40], but fabrication and handling of the corresponding devices are more demanding than for the relatively simple design used here. Lowering the dead times further would require brighter fluorophores than are currently available.) The observation channel is arranged in a serpentine fashion (**Fig. 1a,d**), and its length is chosen such that observation times up to 2 min are easily possible (**Table 1**). Conventional manual mixing combined with a sliding window analysis of the single-molecule fluorescence traces[10,26] is feasible with a dead time and a time resolution of a few minutes[10,26]; as a result, the microfluidic mixing data can be combined with manual mixing data without any gap in accessible times. An additional component of the design that is essential for avoiding the seemingly trivial but very relevant problem of channel blockage was the introduction of microfabricated filters[34,35] (**Fig. 1e**), which prevent dust, protein aggregates or other particles from entering the device and blocking the narrow mixing region. Two-focus fluorescence correlation spectroscopy (FCS)[43] was used to confirm the agreement of the actual flow velocities with the calculated values.

On the basis of 3D finite element calculations (COMSOL Multiphysics), the positions in the observation channel can be converted accurately to times after mixing. Examples for this position-to-time conversion at two typical flow velocities are provided in **Table 2**. The mixing geometry is designed such that small molecules such as salts, denaturants or detergents can be mixed along the 2.5-µm wide mixing region with a dead time of 1 ms and an average flow velocity of ~1 µm ms^{-1} in the observation channel. Note, however, that in spite of the uniform mixing of small solutes,

TABLE 1 | Pressures to be applied to center and side channels for representative mixing conditions.

Average flow velocity, v ($\mu m\ ms^{-1}$)	Mixing ratio, R	Guanidinium chloride concentration in center channel	Guanidinium chloride concentration in side channels	Pressure on center channel (kPa)	Pressure on side channels (kPa)
1.0	1:10	0 M (η = 1 mPa·s)	3.33 M (η = 1.19 mPa·s)	16.8	18.8
1.0	1:10	3 M (η = 1.17 mPa·s)	0 M (η = 1 mPa·s)	16.1	16.1
0.50	1:10	0 M (η = 1 mPa·s)	3.33 M (η = 1.19 mPa·s)	8.3	9.4
0.50	1:10	3 M (η = 1.17 mPa·s)	0 M (η = 1 mPa·s)	8.0	8.1

the concentration of macromolecules under these conditions is not uniform across the early points of the observation channel. If macromolecular components are to be mixed, the flow rates can be reduced such that their complete mixing occurs in the mixing region at the expense of dead time.

TABLE 2 | Position-to-time conversion at two flow velocities for a protein with $D = 8.5 \times 10^{-7}\ cm^2\ s^{-1}$.

Position in observation channel	Time after mixing for: v = 1.0 $\mu m\ ms^{-1}$	Time after mixing for: v = 0.50 $\mu m\ ms^{-1}$
28.75 µm	1.03 ms	2.04 ms
31.75 µm	1.43 ms	2.86 ms
34.75 µm	2.02 ms	4.05 ms
38.75 µm	3.13 ms	6.3 ms
45 µm	5.54 ms	11.31 ms
55 µm	10.7 ms	22.7 ms
70 µm	20.4 ms	45 ms
100 µm	43.1 ms	95.6 ms
150 µm	84.5 ms	182 ms
200 µm	127 ms	269 ms
250 µm	170 ms	356 ms
0.5 mm	0.39 s	0.8 s
1 mm	0.83 s	1.75 s
2 mm	1.76 s	3.72 s
5 mm	4.72 s	9.67 s
10 mm	9.6 s	19.6 s
30 mm	29.5 s	59.3 s
60 mm	59.3 s	118.9 s

See also **Supplementary Table 1**. The microfluidic mixer can cover the time range from milliseconds to minutes. The conversion is derived from 3D time-dependent finite-element calculations for a medium-size protein ($D = 8.5 \times 10^{-7}\ cm^2\ s^{-1}$). Note that shear-augmented diffusion affects the precision of the position-to-time conversion[58]. If precise knowledge of this effect is required, the relationship between diffusion and the laminar flow profile must be calculated in detail[38].

Fabrication of the silicon master. One silicon master can be used for replica molding with PDMS for years if handled with care. The casting dish for the replica molding (drawings provided in **Supplementary Data 2** and **3**) defines the height of the microfluidic devices and at the same time minimizes the risk of damaging the wafer[38]. We describe the photolithographic structuring of the silicon wafer using a specific negative photoresist; however, any similar photoresist that is well established in the clean room used for fabrication should be suitable. Parameters, safety precautions and steps in the protocol will have to be adjusted accordingly. The fabrication of the silicon master requires access to a clean room equipped for photolithography and deep reactive ion etching (DRIE) of silicon and entails a substantial amount of training on the requisite instruments. If only one or a few silicon masters are needed, fabrication by trained clean room staff or a commercial provider may be easier than getting the training required for clean room access and operating the necessary instruments. Although the structures described here can also be produced by soft lithography using negative photoresist, such as SU-8, we use DRIE in silicon because it results in very durable molds with a well-controllable depth that can be used for producing hundreds of replicas without damaging the structures. Photoresist masters have markedly shorter lifespans owing to the relatively weak adhesion of structures with high aspect ratios and small footprints to the silicon wafer. All steps involved in the production of the microfluidic devices after the fabrication of the silicon mold do not require a clean room or clean room expertise and can be performed using commonly available facilities, a standard chemical fume hood and a laminar flow bench (**Supplementary Video 1**).

Device holder. We designed a device holder with a cartridge system that allows rapid and reliable exchange of microfluidic devices and that is optimized for use on a confocal microscope (**Fig. 2** and **Supplementary Video 2**). The holder has a robust and user-friendly interface for loading the device with the sample and buffer solutions and for applying the air pressures needed to drive the flow in the microfluidic channels. The device holder provides access to up to eight inlet or outlet channels. Although for the present microfluidic mixing device only three inlets and one outlet are used, future applications, such as multistage mixing (e.g., 'double-jump' mixing[44]), which require additional channels, may benefit from this layout. Solutions are loaded into 50-µl reservoirs contained in

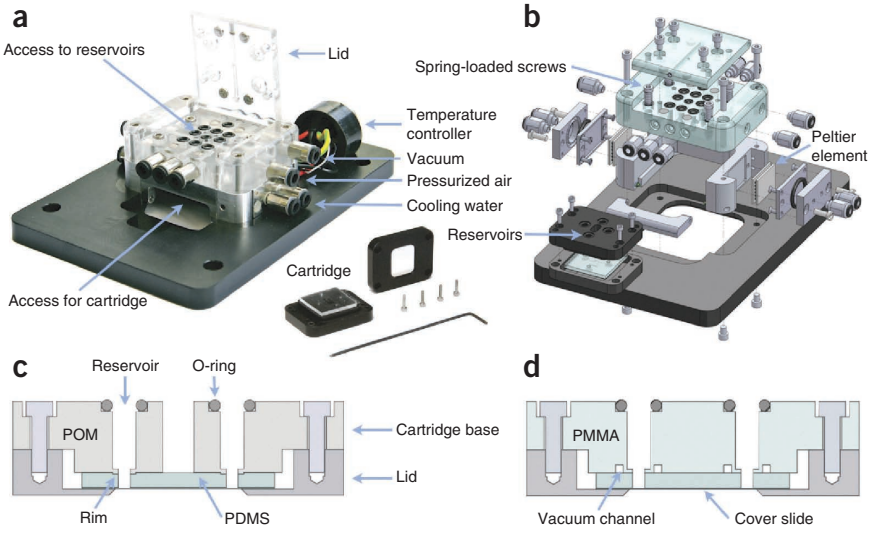

Figure 2 | Cartridge and cartridge holder for mounting the microfluidic devices on the single-molecule instrument. (**a**) Photographic image showing the cartridge holder with open lid and the disassembled cartridge (middle) with the microfluidic device. (**b**) Exploded view of the holder (drawing, for details see **Supplementary Data 4** and **5**). The holder, which mounts on top of an inverted microscope, has connectors for pressurized air, vacuum, and cooling water, as well as electrical connections to the temperature controller. The cartridge, with its 50-µl reservoirs for the inlet solutions can be exchanged without removing any of the connections. To connect the reservoirs with the pressure control system, spring-loaded screws press the cartridge against the (transparent) upper part of the holder. O-ring seals prevent leakage. The reservoirs are accessible from the top by opening the access port lid. Peltier elements mounted to the lower (aluminum) part of the holder can cool or heat the device and are equipped with water-cooled heat sinks. The microfluidic device can be illuminated from the top for inspection with the microscope. (**c**,**d**) Schematic cross-sections of the two types of cartridges that can be used in the holder. In both cases, pressurized air above the reservoirs pushes the solutions through inlet holes into the microfluidic channels, which are confined by the cover slide bound to the bottom surface of the PDMS (not shown). The cartridges differ in their sealing mechanisms. In **c**, the PDMS is pressed against the rims around the reservoir outlets mechanically by tightening the screws. The vacuum cartridge (**d**) has vacuum channels positioned around the outlets instead of rims[45]. Vacuum draws the microfluidic device against the upper part of the cartridge made of PMMA. (**c**) The advantage of mechanical sealing is its simplicity of implementation. However, the mechanical pressure applied to the devices can lead to breakage of the cover slide if the thickness of the PDMS layer is not within specifications. (**d**) In the vacuum cartridge, the cover slide is virtually free of mechanical stress, but a suitable vacuum pump must be available.

a cartridge made of polyoxymethylene (POM) on which the microfluidic device (i.e., the PDMS device bonded to a cover slide) is placed (**Fig. 2**). Holes punched through the PDMS in the inlet post arrays of the device (**Fig. 1a**) connect the cartridge reservoirs with the inlet channels. An aluminum cartridge lid presses the microfluidic device against the rim of the cartridge base, thus forming a tight seal and preventing leakage (**Fig. 2c**). An alternative to the POM cartridges is the use of polymethylmethacrylate (PMMA) cartridges and clamping the microfluidic device with vacuum[45] (**Fig. 2d**). An advantage of the POM cartridges is that they do not require a vacuum line; the PMMA cartridges minimize the risk of breaking the cover glass by the aluminum lid, as the seal is formed by vacuum rather than mechanical pressure. Drawings for both cartridges are provided in **Supplementary Data 4** and **5**, and either can be used in the holder.

For the single-molecule measurements, the cartridge is inserted into the device holder mounted onto the microscope stage (**Fig. 2**). Several assembled cartridges can be prepared to allow for rapid exchange of devices. The upper part of the holder is made of transparent PMMA and allows for illumination of the microfluidic device from above, so that the structures in the mixing region and the observation channel can be visualized by wide-field microscopy. Spring-loaded screws press the cartridge against the PMMA body such that, with the help of O-ring seals (**Fig. 2c**), tight connections are made between the cartridge reservoirs and the air pressure system of the PMMA body. Tubing fittings are provided to connect the pressurized air to the holder. Each reservoir can be pressurized individually. The reservoirs are easily accessible in mid-experiment by opening an access port on top of the holder. During operation of the mixer, the lid is tightly fixed with screws, and O-ring face seals prevent leakage. Precise pressure regulators (<0.2-kPa resolution, e.g., 170 Pa = 0.025 psi for the controllers used in this protocol) are required for fine-tuning the flow velocity in the channels and the mixing ratio.

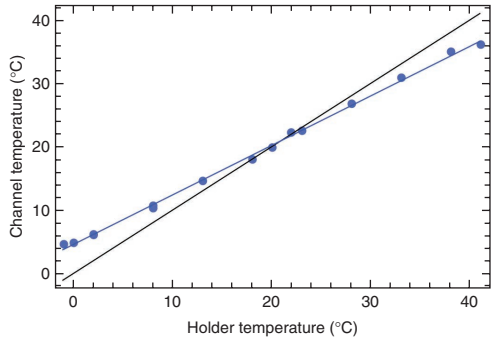

Figure 3 | Calibration curve for the temperature control of the microfluidic device. The temperature inside the observation channel (blue dots) was measured using the temperature dependence of the fluorescence lifetime of rhodamine B. To prevent adhesion to the channel walls, rhodamine B was dissolved in 7.6 M guanidinium chloride. Blue and black lines represent a linear fit to the data and the identity curve, respectively. The lines cross at ~22 °C, the ambient temperature of the laboratory. As the calibration curve depends on the temperature in the room and the heat conduction of the single-molecule instrument, recording a specific calibration curve is required for accurate temperature settings.

Temperature control and calibration. Two water-cooled Peltier elements and a PT100 temperature sensor mounted in the aluminum part of the device holder allow for controlled heating or cooling. As the microfluidic device cannot easily be insulated thermally

from its environment, mainly because of direct contact of the cover slide (170 µm in thickness) to the immersion water of the microscope objective, the temperature inside the microfluidic channel can deviate significantly from the temperature of the holder. Commercially available temperature control for the microscope objective or a custom-built aluminum collar with a water-cooled Peltier element and a temperature sensor can be used to minimize this gradient. However, the deviation between the temperature in the channel and the holder is difficult to eliminate completely and should be calibrated if accurate temperature settings are required. As an example, we determined the temperature in the observation channel 100-µm downstream from the mixing region by measuring the temperature-dependent fluorescence lifetime of rhodamine B[37,46] (**Fig. 3**). As a reference, we measured the solution in an ensemble fluorescence lifetime instrument with accurate temperature control[46]. The temperature in the device depends on the details of the setup and the temperature in the room; we therefore recommend recording calibration curves for the specific system used (Steps 75–81).

The workflow of the entire protocol is shown in **Figure 4**.

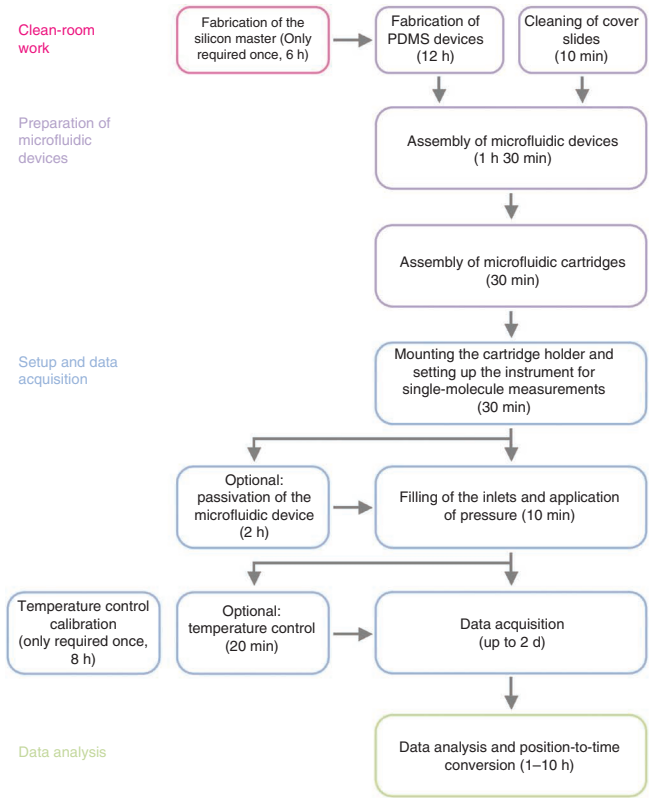

Figure 4 | Workflow diagram of the protocol.

Limitations

The microfluidic mixer is optimized for average flow velocities of ~1 µm ms^{-1} and a mixing ratio of 1:10 (center inlet to side inlets). Different mixing ratios (1:20 to 1:5) and average flow velocities (0.5 to 2 µm ms^{-1}) can be achieved by changing the pressures applied to the inlets[38]. However, outside this range of values, controllability of the flow will gradually decrease; leakage can result at very high driving pressures; and the onset of mixing can shift owing to the diffusion of solutes from the mixing region into the inlet channels at very low flow rates required for extreme mixing ratios. Although the mixer is optimized for the diffusive mixing of small molecules (e.g., salts or denaturants), it can also be used for mixing larger molecules such as to investigate the association of biological macromolecules[26]. The diffusion coefficients of the components can be used to estimate the flow velocities to be used. The driving pressures must then be adjusted so that diffusive mixing is complete during passage of the narrow mixing region (**Fig. 1b**). As the mixing time is inversely proportional to the diffusion coefficient of the solutes to be mixed[38], the earliest times after mixing accessible in the device will increase accordingly.

The current system can be used for temperatures up to 37 °C. This upper limit is related mostly to the temperature range specified for the microscope objectives used in single-molecule spectroscopy. Measurements above 37 °C require optics that can be used at higher temperatures, but the design and materials of the mixing system itself lend themselves to a much wider temperature range.

MATERIALS

Reagents

Fabrication of the silicon master

- Negative photoresist (Futurex, cat. no. NR7-1000P) **! CAUTION** Negative photoresist is flammable. Wear protective clothing, goggles and appropriate protective gloves while handling it. Wear appropriate respirator when ventilation is inadequate. Store it in a cool, dry, well-ventilated area in a tightly closed container, away from incompatible substances. Keep it away from heat and flame.
- Resist developer (Futurex, cat. no. RD6) **! CAUTION** Resist developer is an alkaline liquid. Wear goggles, suitable gloves (butyl rubber gloves) and protective clothing while handling it. Store it in a tightly closed plastic container in a well-ventilated place. Store it away from incompatible materials.
- Resist remover (Futurex, cat. no. RR4) **! CAUTION** Resist remover is a combustible liquid. Wear goggles, suitable gloves (butyl rubber gloves) and protective clothing while handling it. Store it in a cool, well-ventilated place. Store it away from incompatible materials.
- Acetone
- Isopropanol
- Distilled water

Fabrication of the microfluidic devices

- Trimethylchlorosilane (TMCS; Sigma-Aldrich, cat. no. 92361) **! CAUTION** TMCS is highly flammable, corrosive and toxic. It reacts violently with water. Wear suitable protective clothing, face and eye protection, and gloves (nitrile rubber) while handling it. Store it tightly closed in a dry and well-ventilated place, and handle it only in the fume hood.
- Polydimethylsiloxane (PDMS; RTV 615 kit, Momentive) is used for replica molding. Store it at 4 °C and use it within the shelf life recommended by the manufacturer.
- Cleaning agent (e.g., Deconex, Borer Chemie)
- Distilled water

Surface passivation of the microfluidic devices

- BSA (Albumin Fraktion V, Art. T844.1, Carl Roth)
- PEG (PLL(20)-g[3.5]-PEG(2), Susos) Tween-20 (Pierce). Aliquots can be used for many months if stored at −20 °C.

EQUIPMENT

Fabrication of the silicon master

- Silicon wafer, 100-mm diameter, 500 ± 5 µm in thickness, one side or both sides polished, any orientation

- Wafer box for 100-mm wafers
- Chrome mask (produced by Compugraphics Jena on the basis of the drawing provided in **Supplementary Data 1**; can be viewed using the free software KLayout)
- Hexamethyldisilazane (HMDS) station
- Mask aligner (Carl Suess MA6)
- Spin coater (Suess RC 5 GYRSET)
- Hot plate
- Quick-dump rinser
- Rinser dryer
- Inductive coupled plasma for reactive ion etching (STS ICP)
- Surface profiler (Tencor P10)
- Wafer tweezers
- Polytetrafluoroethylene (PTFE) dish
- Light microscope for wafer inspection in the clean room

Casting of the microfluidic devices in PDMS

- Casting dish (technical drawings and CAD files provided in **Supplementary Data 2** and **3**)
- Balance
- Scalpel
- Glass crystallization dish
- Parafilm
- PMMA template for punching inlet holes (drawings provided)
- Puncher, 1.5-mm (Harris Uni Core 15075, Ted Pella)
- CleanWipe swab (Foamtec Internation, HT1002)
- Fused silica cover slides, 25 mm × 25 mm (Esco Products, cat. no. R425025)
- Cleaning agent (e.g., Deconex, Borer Chemie)
- Coverslip PTFE mini-rack (Invitrogen, cat. no. C-14784)
- PTFE tweezers
- Wafer tweezers
- Plasma cleaner (FEMTO, Diener)
- Oven (60 °C)
- Light microscope for device inspection (Olympus MX51)

Hardware for microfluidics experiments

- Cartridge(s) for holding microfluidic devices (technical drawings and CAD files provided in **Supplementary Data 4** and **5**)
- Temperature-controlled cartridge holder (technical drawings and CAD files provided in **Supplementary Data 4** and **5**)
- Tubing fittings (push-in fittings, Legris, cat. no. 3101 0409)
- Flexible polyurethane tubing, outer diameter 4 mm, inner diameter 2.5 mm 4 × 2.5 (clear, cat. no. 1025U04R08; blue, cat. no. 1025U04R04; yellow, cat. no. 1025U04R05, Legris)
- Electropneumatic pressure transducers (Marsh Bellofram, cat. no. 3110)
- Pressure gauge (WIKA, cat. no. 611.10)
- Vacuum pump (optional; LABOPORT N 816.3, KNF)

Hardware for temperature control (optional)

- Temperature controller capable of driving Peltier elements (Thorlabs, cat. no. TED4015)
- Temperature control system for the objective (depends on the microscope and objective used)
- PT100 temperature sensor (Honeywell, cat. no. HEL-705-T-0-12-00)
- Peltier elements (Uwe Electronic, cat. no. UEPT-1RE-023-080M125S)

! CAUTION High currents are used to drive the Peltier elements. Connect the temperature-controlled cartridge holder to the ground.

- Cooling water
- Thermal decoupling of the objective (Thorlabs, thermally stable adaptors, cat. nos. SM1A4TS and SM1A3TS)

Data acquisition

- Inverted microscope (Olympus IX71)
- Confocal single-molecule instrumentation (e.g., MicroTime 200, PicoQuant)

REAGENT SETUP

BSA solution Dissolve the lyophilized protein in double-distilled water, filter it through a 450-nm PVDF membrane and store 50-µl aliquots at −20 °C for several months.

PEG Dissolve PEG in double-distilled water and store 50-µl aliquots at −20 °C for several months.

PROCEDURE

Fabrication of the silicon master (photolithography and reactive ion etching) ● TIMING 6 h

1| Expose a clean and dry silicon wafer (diameter 100 mm, thickness 500 ± 25 µm) to HMDS as an adhesion promoter for 30 s. **! CAUTION** Wear protective goggles, suitable gloves and protective clothing when working with HMDS, photoresist, developer and remover. Use these reagents only in a well-ventilated area, and obey the clean room guidelines and the manufacturers' MSDS.

2| Transfer the wafer to the spin coater using wafer tweezers, and then switch on the vacuum to clamp the wafer.

3| Slowly pipette ~3 ml of negative photoresist (e.g., Futurex NR7-1000P) onto the center of the wafer. Avoid introducing air bubbles.

4| Spin-coat the wafer with the negative photoresist. Accelerate the spinner to 700 r.p.m. at 500 r.p.m. s^{-1} and spin for 5 s, and then accelerate to 1,700 r.p.m. at 1,000 r.p.m. s^{-1} and spin for 35 s. This should result in a layer of photoresist of ~1.5 µm in thickness.

5| Prebake the wafer at 150 °C for 60 s on a hot plate. Put the wafer on a PTFE dish to cool down.

6| Load the chrome mask and wafer into the mask aligner.

7| Expose the photoresist to UV light. Choose exposure time according to the specifications of the photoresist (e.g., Futurex NR7-1000P: 7 × 10 s at 4.2 mW cm^{-2} at 365 nm). If possible, use hard or vacuum contact between the mask and the wafer to achieve best resolution.

8| Postbake the wafer at 100 °C for 60 s on a hot plate. Put the wafer on a PTFE dish to cool down.

9| Develop the photoresist by gently moving the wafer in developer (e.g., 5:1 Futurex RD6: H_2O) for ~3 min.
▲ CRITICAL STEP Make sure all unwanted photoresist is removed from the wafer without overdeveloping the structures.

10| Carefully rinse the wafer with distilled water. Clean it in a quick-dump rinser and in a rinser dryer.

11| Transfer the patterned wafer into an instrument for inductive-coupled plasma DRIE (Bosch process). Etch the silicon wafer 10 µm deep according to the specifications of your instrumentation.

12| Remove residual photoresist with resist remover (e.g., Futurex RR4) or organic solvents (e.g., acetone). Clean the wafer with acetone, isopropanol and distilled water in a quick-dump rinser, and then dry it in a rinser dryer.

13| Measure the height of the structures using a surface profiler (e.g., Tencor P10).

14| Place the etched silicon master in a wafer box and note the date of fabrication, the heights of the features and other relevant parameters.

■ **PAUSE POINT** Once the wafer is stored in the wafer box, it can be transferred from the clean room to the laboratory where the device casting will be performed. We recommend opening the wafer box only in a laminar flow bench to avoid contamination by dust. If it is handled with care, the silicon master can be used for years.

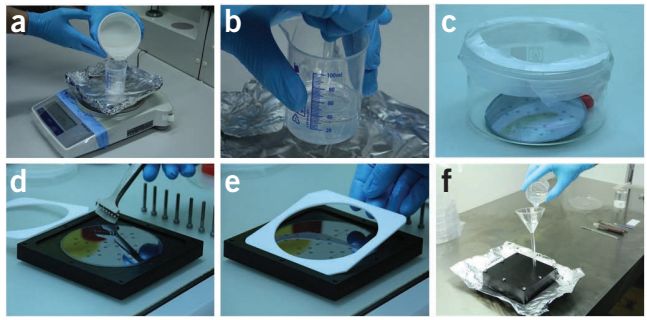

Figure 5 | Casting the PDMS devices. (**a**) Weigh in PDMS RTV615 components A and B in a 10:1 ratio. (**b**) Mix the PDMS by stirring with a 1-ml pipette tip and degas the mixture in a vacuum desiccator. (**c**) Expose the master wafer to TMCS in the fume hood for 30 min. (**d**) Transfer the wafer to the bottom part of the casting dish using wafer tweezers and align the wafer flat with one of the edges of the casting dish. (**e**) Insert the PTFE spacer, which defines the height of the PDMS replica. (**f**) Fasten the lid of the casting dish with eight M4 screws and pour the degassed PDMS in the holder using a funnel; cure in an oven at 60 °C for 10 h.

Casting of the PDMS devices (replica molding) ● **TIMING 12 h**

15| Wash a 50-ml plastic beaker and a funnel with distilled water, and then dry them with compressed air.

16| Weigh in components A and B of the PDMS kit in a 10:1 ratio by weight (e.g., 25 g and 2.5 g, respectively; **Fig. 5a**). Mix both components by stirring gently with a 1-ml pipette tip (**Fig. 5b**).

17| Degas the mixed viscous solution in a vacuum desiccator. Bubbles form and start to rise. Release the vacuum frequently to collapse the bubbles until no more bubbles form (~15 min).

! **CAUTION** TMCS is highly corrosive and should not come in contact with metals. To minimize the experimenter's exposure to TMCS, Steps 19 and 20 should be performed in a fume hood and while wearing suitable protective clothing. TMCS should not be handled outside the fume hood (including the laminar flow bench).

18| To prevent PDMS adhesion, expose the etched silicon master to TMCS for 30 min in a fume hood by placing the wafer in a crystallization dish and adding ~1 ml of TMCS in a small container. Seal the crystallization dish with Parafilm (**Fig. 5c**).

19| Mount the silicon master in the casting dish in the fume hood. Place the wafer in the recess of the base plate and align the wafer flat with one of the edges of the base plate (**Fig. 5d**). Insert the PTFE spacer in the base plate on top of the wafer (**Fig. 5e**), and then close the casting dish with the lid using M4 screws.

20| Transfer the casting dish to the flow bench and pour the degassed PDMS into the inlet hole of the lid using a funnel (**Fig. 5f**).

21| Once PDMS emerges from the overflow ports, remove the funnel and cure the PDMS in an oven at 60 °C for 10 h.

22| Transfer the casting dish to the flow bench and let it cool to room temperature (~20 °C).

23| Clean a disposable 15-cm polystyrene Petri dish with distilled water and dry it with compressed air.

24| Remove excess PDMS from the lid using a scalpel (**Fig. 6a**). Disassemble the casting dish by loosening the M4 screws and opening it with a twisting motion (**Fig. 6b**). The PDMS cast will stick to the lid of the casting dish (**Fig. 6c**). Carefully cut the PDMS from the overflow ports with a scalpel (**Fig. 6d**). Transfer the PDMS cast into the Petri dish with the channel side facing down (**Fig. 6e**). Cut out 25-mm squares with a scalpel along the corresponding reference marks (**Fig. 6f**).

▲ **CRITICAL STEP** Holes punched into the PDMS for inlets and outlets should exactly match the reservoir hole pattern in the microfluidic cartridges. The PMMA template with holes with the correct spacing can be used to precisely position the puncher.

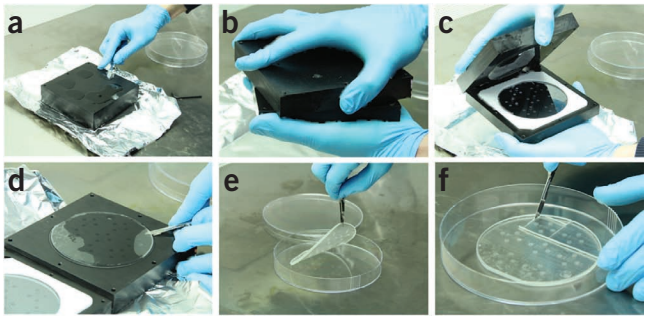

Figure 6 | Processing the PDMS cast. (**a**) Remove excess PDMS from the holder using a scalpel. (**b**) Loosen the top part of the holder with a twisting motion and open it. (**c**) The PDMS will stick to the lid of the casting dish. (**d**,**e**) Release the PDMS from the holder with a scalpel (**d**) and transfer it to a clean Petri dish with the channel side facing down (**e**). (**f**) Cut the PDMS into squares of 25 mm × 25 mm with the scalpel.

25| Align the punching template with the structures on the PDMS device. Punch inlets and outlets in the post arrays using a 1.5-mm puncher (**Fig. 7a**).
■ **PAUSE POINT** When they are protected from dust, PDMS devices can be stored for months in a clean Petri dish until they are bonded to the fused silica cover slide.

Cleaning cover slides ● TIMING 10 min
26| Place a cover slide in the PTFE mini rack and boil it in a cleaning agent (e.g., 10% (vol/vol) Deconex) for 30 s. Carefully rub the cover slide with a clean-room swab and wash it with distilled water (**Fig. 7b**).

27| Store the cover slides in the PTFE mini rack in distilled water and transfer them to the flow bench. Seal the beaker with Parafilm.
■ **PAUSE POINT** The cover slides can be stored, submerged in water, until they are bonded to the PDMS devices.

Assembly of the microfluidic devices ● TIMING 1 h 30 min
▲ **CRITICAL** Assembly of the microfluidic devices should be performed in a laminar flow bench to minimize contamination by dust and resulting leakage (**Supplementary Video 1**).

28| Dry the cover slide with compressed air (**Fig. 7c**). Place the cover slide and the PDMS device, with the channel side facing up, in a plasma cleaner (**Fig. 7d**).

29| Evacuate the plasma chamber and establish a stable flow of air (70–90 cm^3 min^{-1}). Expose the PDMS and the cover slide to oxygen plasma for 30 s (e.g., at 25% power for the Diener FEMTO, diameter 100 mm, 100 W, 40 kHz). Optimal settings of flow rate, power and exposure time depend on the plasma cleaner used and may have to be optimized to achieve optimal bonding.

30| Vent the chamber and retrieve the PDMS device and the cover slide. Place the PDMS, with the channel side facing up, on a clean piece of PTFE and position the cover slide on the channel side of the PDMS device (**Fig. 7e**). Gently apply pressure with a clean-room swab (**Fig. 7f**). Let the microfluidic device bond for 1 h.

31| Inspect the bonded microfluidic device under a microscope. Discard devices that have inclusions (e.g., dust particles) in the channels or other defects.
■ **PAUSE POINT** Although the microfluidic devices are best used immediately after assembly because the high hydrophilicity after bonding simplifies loading the channels with aqueous solutions, they can be used for up to 1 week after assembly. We recommend binding only the number of devices required for use within a few days.

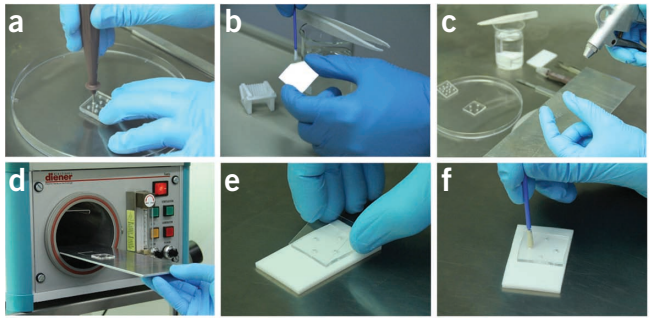

Figure 7 | Assembly of the microfluidic device. This procedure is demonstrated in **Supplementary Video 1**. (**a**) Align the PMMA template with the PDMS device and punch holes using the 1.5-mm puncher. (**b**) Clean the cover slides by boiling them in detergent; rub them with a clean-room swab under distilled water. We recommend the use of fused silica cover slides because of their low luminescence background[38]. If the background requirements of the experiment are less stringent, glass cover slides are an economical alternative. Store the cover slides in distilled water. (**c**,**d**) Dry the cover slide with pressurized air (**c**) and expose the cover slide and PDMS to oxygen plasma (**d**). (**e**,**f**) Align the cover slide with the PDMS chip (**e**) and gently apply pressure with a clean-room swab (**f**). Let the chips rest for 1 h.

Assembly of the microfluidic cartridges ● TIMING 30 min
32| Clean the cartridge by sonication in cleaning agent (e.g., 10% (vol/vol) Deconex) for 10 min and thoroughly rinse it with distilled water. Dry the cartridge with compressed air.

33| While working at the flow bench, place the microfluidic device on the cartridge, put the lid on the device and carefully turn the cartridge over. Make sure the holes in the

microfluidic device are well aligned with the cartridge inlet reservoirs. Fasten the lid by gently tightening the four M2 screws hand-tight (**Supplementary Video 2**).
▲ **CRITICAL STEP** The seal between the microfluidic device and the cartridge depends on how tightly the screws are fastened. Tightening the screws in an uneven manner or too quickly can break the cover slide. Note that the thickness of the PDMS device, as determined by the depth of the casting dish, is designed to achieve an optimal seal in the cartridge.
? TROUBLESHOOTING

34| (Optional) If a vacuum cartridge is used, the cartridge is assembled in the same way. In addition, apply vacuum (20 kPa) to the cartridges for 30 min to increase adhesion between the PDMS device and the PMMA cartridge. Using vacuum cartridges can help prevent cover slide breakage (**Fig. 2d**).

35| Either load the cartridge with buffer and sample solution for direct use or store it in the flow bench until required to minimize contamination by dust.
■ **PAUSE POINT** Several cartridges can be assembled and stored in the flow bench until they are needed for the experiment. Once assembled, they should be used within a few days.

Mounting the cartridge holder and setting up the instrument for single-molecule measurements ● TIMING 30 min
36| Put a drop of immersion water on the microscope objective (note that the objective lens is not readily accessible once the cartridge holder is mounted). For measurements of more than a few hours, it is helpful to seal the objective with a suitable rubber gasket to avoid evaporation of the immersion water.

37| Move the microscope objective to the lowest position.

38| Mount the cartridge holder on the microscope stage (see **Supplementary Data 4** and **5**). The baseplate for the holder (drawing, see appendix) is designed to be inserted in a Märzhäuser SCAN IM motorized microscope stage for an OLYMPUS IX71 inverted microscope. The base plate might have to be modified if a different microscope stage is used.

39| Attach the tubing (**Fig. 8a** and **Supplementary Video 2**) for applying pressurized air to the center and to the two side inlets. The pressure used to drive the solutions through the channels is controlled by electropneumatic pressure transducers and monitored by pressure gauges.

40| (Optional) For using the vacuum cartridges, additionally attach the corresponding connection to a vacuum pump.

41| Insert the cartridge into the holder (**Fig. 8b** and **Supplementary Video 2**). Fasten the cartridge with the four spring-loaded screws until they are hand-tight.

42| The reservoirs in the cartridge can be accessed by opening the access port lid of the cartridge holder for filling or replacing buffer and sample solutions (**Fig. 8c** and **Supplementary Video 2**). Magnets keep the lids closed. In addition, four screws can be used to fasten the lid.

43| (Optional) If a vacuum cartridge is used, switch on the vacuum pump.

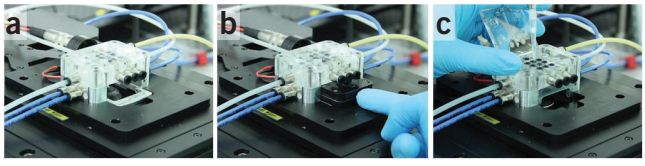

Figure 8 | Loading the cartridge holder. This procedure is also demonstrated in **Supplementary Video 2**. (**a**) Mount the cartridge holder on the microscope, attach the tubing for pressurized air (blue), cooling water (white) and vacuum (yellow), and then connect the Peltier elements to the temperature controller. (**b**) Move the microscope objective to the lowest position, load the cartridge and fasten it with four screws. (**c**) Open the lid to load solutions with a pipette, switch on the laser and move the microscope objective into contact with the cover slide of the device.

44| Center the cartridge holder over the microscope objective by moving the microscope stage.

45| Use the ocular or a wide-field camera to inspect the microfluidic channels with the microscope. The device can be illuminated from the top. Move the field of view along the channels and make sure that the channels are free of any particles or dust that could cause channel blockage. Finally, bring the mixing region into view (**Fig. 9a**).

46| Switch on the excitation laser of the single-molecule instrument. Adjust the laser power to the desired level (e.g., 100 μW).

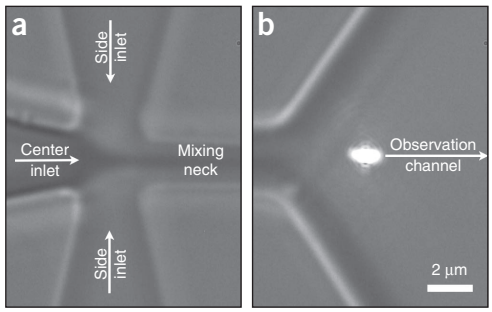

Figure 9 | Wide-field microscopy images of the mixing device in operation. (**a**) Hydrodynamic focusing is visible in the mixing region if the difference in refractive index between the center and side inlet solutions (0 and 3.33 M guanidinium chloride, respectively, in this example) is sufficiently large. It is advantageous to check the symmetry of the flow before data acquisition. (**b**) The tapered part of the observation channel with the back-reflection of the focused laser beam.

47| To position the confocal volume in the mixer, select the light path and the filters of the single-molecule instrument such that both the confocal laser spot (back-reflection from the top surface of the cover slide) and the channels of the microfluidic device can be imaged on the internal camera of the instrument.
! CAUTION For safety reasons, the single-molecule instrument used in this protocol (MicroTime 200, PicoQuant) does not allow laser light to be observed through the eyepiece of the microscope but only on an internal charge-coupled device (CCD) camera. Other instrumentation might be set up differently, in which case great care must be taken to prevent damage to the eyes.
? TROUBLESHOOTING

48| Focus the laser beam to the upper surface of the cover slide.

Passivation of the microfluidic device (optional) ● TIMING 2 h
▲ CRITICAL In some cases, surface adhesion of the sample molecules to the channel walls is too strong without surface passivation. Coating the microfluidic channels with BSA or PEG helps to reduce this effect.

49| Load 50 µl of a mixture of BSA and PLL-PEG in distilled water (10 mg ml^{-1} BSA, 0.2 mg ml^{-1} PLL-PEG) into the center channel reservoir, and load distilled water into the side channel reservoirs.

50| Close the lid of the cartridge holder, tighten the screws and apply 20 kPa of pressurized air to the center channel and 3.5 kPa to the side channels for 30 min to expose the walls of the sample and the outlet channel to the passivation agent.
? TROUBLESHOOTING

51| Remove the BSA/PLL-PEG from the center channel reservoir and wash the reservoir three times with 60 µl of distilled water.

52| Flush all channels with distilled water for ~1.5 h (20 kPa center channel, 3.5 kPa side channels) or until the background count rate decreases to a level low enough for single-molecule detection (see Steps 64–70).

Filling of the inlets and application of pressure ● TIMING 10 min
▲ CRITICAL In order to calculate the pressures required to drive the flow, it is necessary to know the viscosities of the solutions in the center inlet, side inlets and observation channel, represented as η_{center}, η_{side} and η_{obs}, respectively. Either viscosities can be taken (or interpolated) from tabulated values[47,48] or, preferably, they can be determined in a viscometer for the specific solutions and temperatures used.

53| Load 10 and 50 µl of the solutions to be mixed into the center and side channel reservoirs, respectively (**Fig. 8c** and **Supplementary Video 2**). Include mild detergent (e.g., 0.001–0.01% (vol/vol) Tween-20) to reduce sample adhesion to the channel walls if required. Close the access port lid and tighten the screws. For single-molecule detection, the concentration of fluorescently labeled sample should be chosen such that its final concentration after mixing is ~20–100 pM.

54| Choose suitable values for the mixing ratio, $R = Q_{ci}/Q_{obs}$ (where Q_{ci} and Q_{obs} are the volume flow rates in the center inlet channel and the observation channel, respectively)[38], and the mean flow velocity, v, in the observation channel. Note that the mixer is optimized for values of $R = 0.1$ and $v = 1$ µm ms^{-1}.

55| Calculate the pressure to be applied to the inlet channels (p_{center} and p_{side}) according to a lumped impedance model[38] using the following equations:

$$p_{center} = 50.42\,nm^{-1} \times R\,v\,\eta_{center} + 10.03\,nm^{-1} \times v\,\eta_{obs}$$

$$p_{side} = 6.63\,nm^{-1} \times (1-R)\,v\,\eta_{side} + 10.03\,nm^{-1} \times v\,\eta_{obs}$$

See **Table 1** for examples.

56| Apply the pressures calculated. To avoid leakage, do not open the valves too quickly. If possible, monitor the filling of the channels using the microscope to ensure fluid entry in all inlet channels and the absence of bubbles.
? TROUBLESHOOTING

57| If the refractive indices of center and side inlet channel solutions are different, symmetric hydrodynamic focusing of the center stream should be visible (**Fig. 9a**) and can be used to monitor flow stability.

Temperature control (optional) ● TIMING 20 min
▲ CRITICAL As mentioned in the INTRODUCTION, we advise heating or cooling the microscope objective to the same temperature as the cartridge holder. Adaptors with low heat conductivity can be used to thermally decouple the objective from the microscope body.

58| Connect the cartridge holder to the cooling water circuit.

59| Connect the Peltier elements and the PT100 sensor to the temperature controller.

60| Focus the laser to the top surface of the cover slide and observe the back reflection (**Fig. 9b**).

61| Set the temperature controllers for the microscope objective and the holder to the desired temperature. Use the calibration curve in **Figure 3** or your own temperature calibration to convert the temperature reading to the actual temperature in the microfluidic channel.

62| The image of the laser spot will move out of focus as the temperature changes, mainly because of the changes of the refractive index of the immersion water. Readjust the *z* position of the objective lens to keep the laser spot focused.

63| After ~15 min, when the temperature has equilibrated across the system, the image of the laser focus will become stable and measurement can begin.

Data acquisition ● TIMING up to 2 d
64| Focus the laser to the upper surface of the cover slide (i.e., the lower surface of the observation channel) (**Fig. 9b**).

65| Move the microscope stage to position the focus at the location along the observation channel desired for the measurement. Small ticks spaced at 25-µm intervals and large-numbered ticks spaced at 100-µm intervals next to the channel can be used to identify the correct position along the channel (**Fig. 1c**). The distances are given with respect to the center of the mixing junction.

66| When the correct position in the horizontal plane of the device is reached, adjust the position of the laser focus to the lower surface of the channel. Move the laser focus up; after 10 µm of travel, the reflection of the laser from the upper channel wall should become visible. Position the laser spot in the middle of these two reflections to center the confocal volume in the channel along the vertical axis.

67| Switch off the illumination light to avoid overexposure of the single-photon detectors, and cover the cartridge holder to avoid room light from interfering with the measurement (e.g., using cardboard or some other opaque material).

68| Prepare the single-molecule instrument for data acquisition: switch on detectors, adjust the light path, open the shutters and so on.

69| Record data (e.g., for 30 min). Bursts of fluorescence from single molecules passing through the observation volume should be detectable. Adjust the concentration of fluorescently labeled sample if required.
? TROUBLESHOOTING

70| Repeat Steps 64–69 at different positions along the channel, corresponding to different times after mixing.
? TROUBLESHOOTING

Data analysis and position-to-time conversion ● TIMING 1–10 h
71| Import data with suitable software.

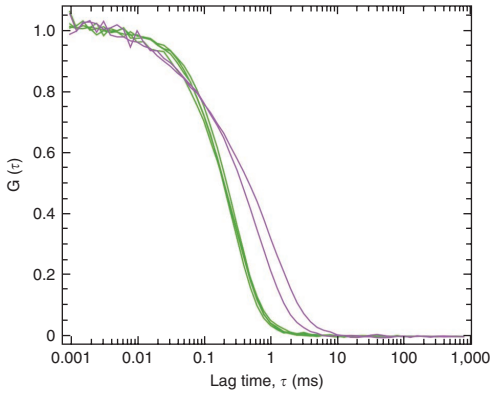

Figure 10 | Normalized FCS curves, G(τ), of fluorescently labeled protein passing through the confocal volume positioned in the observation channel. The decay time of the correlation curve is determined both by the diffusion coefficient and the flow velocity of the fluorescent species. With stable flow, the FCS curves overlay for all lag times (τ) (green lines). However, if the flow velocity decreases (e.g., as a result of channel blockage by dust or protein aggregates), the FCS curves will shift to longer decay times (purple lines). This is an example from a measurement with a microfluidic device that showed signs of channel blockage after several hours of use. Note that flow velocities can be determined quantitatively from FCS data if the shape of the confocal volume is known precisely[51]. More accurate values can be obtained from two-focus FCS[43,57], which was also used for the present mixing device to confirm the calculated flow rates experimentally.

72| Analyze the data according to your needs. For example, if the sample molecules are labeled with a FRET dye pair, identify fluorescence bursts; apply corrections for detection efficiency, cross-talk and acceptor direct excitation; and then generate transfer efficiency histograms or related output[1,49,50].

73| FCS curves calculated from the data acquired are very useful for monitoring the stability of the flow (**Fig. 10**). The flow velocity is expected to be constant along the central axis of the observation channel, with the exception of the entrance length. A drop in flow velocity (e.g., caused by blocked channels or leakage) results in a shift of the correlation curves toward longer lag times. We recommend inspecting the FCS curves after each measurement. By using suitably calibrated equipment, even absolute flow rates can be extracted[43,51] and used to monitor the performance of the device.

74| **Table 2** provides the position-to-time conversion. Here we assume that the sample molecules were supplied to the center inlet. The table summarizes the position-to-time conversion at two commonly used flow velocities. **Supplementary Table 1** provides a more complete set of conversion points.

Temperature control calibration (optional) ● **TIMING 8 h**

▲ **CRITICAL** The temperature dependence of the fluorescence lifetime of rhodamine B[37,46] is used to determine the temperature in the microfluidic channels.

75| Fill inlet channels with 1 μM rhodamine B dissolved in 7.6 M guanidinium chloride and 0.01% (vol/vol) Tween-20.

76| Apply 15 kPa of pressurized air to the center and side channel inlets.

77| Set the holder temperature, T_{holder} (Steps 58–63).

78| Record fluorescence lifetime data by following Steps 64–69.

79| Determine the fluorescence lifetime $\tau_{channel}$ from the data.

80| The temperature inside the channel can be calculated using

$$T_{channel} = 135.42\ ^{\circ}C - 80.42\ ^{\circ}C\left(\frac{\tau_{channel}}{ns}\right) + 24.94\ ^{\circ}C\left(\frac{\tau_{channel}}{ns}\right)^2 - 3.73\ ^{\circ}C\left(\frac{\tau_{channel}}{ns}\right)^3$$

This polynomial approximation is derived from fluorescence lifetime measurements in a temperature-controlled cuvette and is valid in 7.6 M guanidinium chloride for the temperature range from 1–70 °C.

81| Repeat Steps 77–79 for different holder temperatures.

? TROUBLESHOOTING

Troubleshooting advice can be found in **Table 3**.

TABLE 3 | Troubleshooting table.

Step	Problem	Solution
33	Cover slide breaks while mounting the device in the cartridge	Thickness of the device might be higher than the gap in the cartridge. Verify the dimensions of the casting dish. Alternatively, try tightening the screws more gently or use vacuum cartridges
47	The laser spot and microfluidic device are not visible at the same time on the camera of the single-molecule instrument	Check that the light path is selected correctly. Vary the relative intensities of the laser and the light from the microscope lamp to obtain suitable contrast
50, 56	Leakage of fluid between the device and the cartridge	Avoid sudden jumps in pressure. If possible, ramp up the pressure slowly when filling the channels with fluid. Freshly prepared devices are filled more easily than old devices When loading the vacuum cartridge with solutions on the instrument, avoid pushing the tip of the pipette against the microfluidic device. In addition, dust or other contamination reduces the adhesion between the PDMS device and the vacuum cartridge
	The set pressure and pressure gauges do not match, or the indicator on the pressure gauge is vibrating	Leakage might be present in the system. Check the push-in fittings and the fit of the cartridge in the holder. If necessary, fix the lid of the cartridge holder with the screws
	A hissing sound can be heard when applying pressure	Check that the cartridge is inserted in the right orientation Tighten the screws that press the cartridge against the cartridge holder and the screws of the lid
69	Lower fluorescence signal in the observation channel than expected	Inspect inlet channels and mixing region for channel blockage (**Figs. 1c** and **9**). Asymmetric hydrodynamic focusing is an indication of particles clogging the channels. Replace the microfluidic device Protein might adhere to the channel walls. Follow the passivation steps before loading the protein in the mixer Increase the protein concentration in the sample inlet Increase the concentration of Tween-20 up to 0.01% (vol/vol)
	High background from PDMS	Close the shutters and increase the laser power (e.g., tenfold) to bleach the PDMS at this position for 10 min. Decrease the laser power to value of choice before opening the shutters again
70	The laser spot cannot be focused at positions toward the end of the outlet channel	The objective lens might be touching the rim of the base plate. If reaching these positions is essential, the aperture in the base plate needs to be modified

● TIMING

Steps 1–14, fabrication of the silicon master (photolithography and reactive ion etching): 6 h
Steps 15–25, casting of the PDMS devices (replica molding): 12 h
Steps 26 and 27, cleaning cover slides: 10 min
Steps 28–31, assembly of the microfluidic devices: 1 h 30 min
Steps 32–35, assembly of the microfluidic cartridges: 30 min
Steps 36–48, mounting the cartridge holder and setting up the instrument for single-molecule measurements: 30 min
Steps 49–52, passivation of the microfluidic device (optional): 2 h
Steps 53–57, filling of the inlets and application of pressure: 10 min
Steps 58–63, temperature control (optional): 20 min
Steps 64–70, data acquisition: up to 2 d
Steps 71–74, data analysis and position-to-time conversion: 1–10 h
Steps 75–81, temperature control calibration (optional): 8 h

ANTICIPATED RESULTS

The microfluidic mixer can be used to observe kinetics on timescales from milliseconds to minutes. To demonstrate this functionality, we present results of two mixing experiments: the millisecond-scale unfolding of the B-domain of protein A

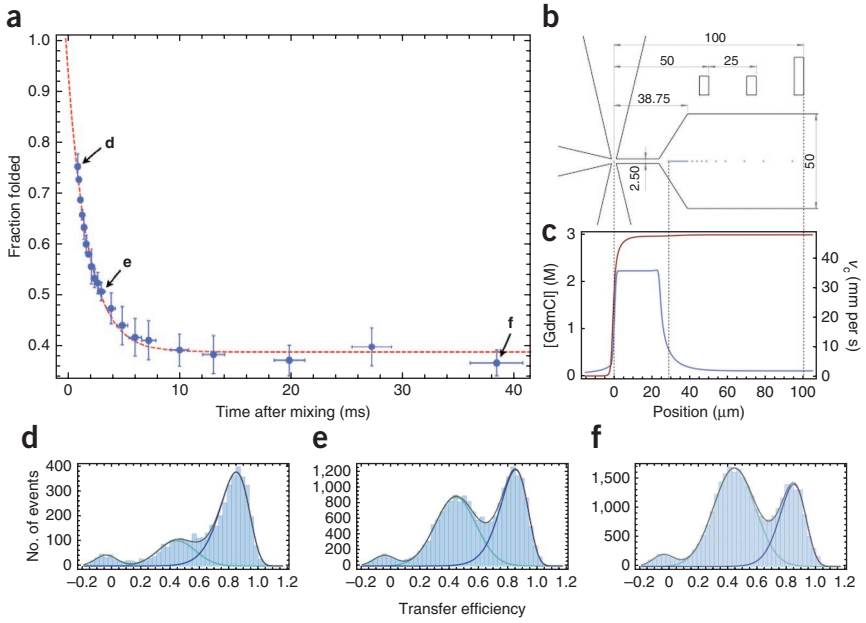

Figure 11 | Unfolding kinetics of BdpA upon mixing with denaturant. Native BdpA in the center inlet was mixed with 3.3 M guanidinium chloride (GdmCl) from the side inlet channels. (**a**) The fraction of folded population (blue data points) was determined from fits to the transfer efficiency histograms and plotted as a function of time after mixing. Three sets of measurements were averaged; vertical error bars indicate the resulting estimates of s.d. The horizontal error bars were calculated assuming an uncertainty of 0.5 μm in positioning the laser focus, and flow velocity variations of 5%. The data were fitted with a single exponential decay (dashed red line). (**b**) Dimensioned drawing of the mixing region and the beginning of the observation channel. Dimensions are given in micrometers. Small dots in the observation channels correspond to the positions where data in **a** were recorded. (**c**) Concentration of denaturant (red line) and flow velocity (blue line) along the center streamline, v_c, derived from 3D finite-element calculations for the pressures and viscosities used in the experiment. The first measurement points are within the hydrodynamic entrance length[38], in which the flow velocity is higher than in the fully developed flow in the observation channel. (**d**–**f**) Representative transfer efficiency histograms measured at positions 28.75 μm (**d**), 38.75 μm (**e**) and 92.75 μm (**f**). Solid lines in **d**–**f** are global fits to the transfer efficiency histograms. To resolve the fast folding dynamics of the sample, transfer efficiencies were calculated from photon counts in time bins of 0.25 ms in length. Only time bins with more than 25 detected photons were used. The acquisition times were 30 min for each histogram. The smaller number of events obtained within the entrance length is due to the reduced light collection efficiency[38] and higher flow velocities in this part of the channel (**c**).

(BdpA)[17,52,53] upon mixing with denaturant and the conformational changes of ClyA, a pore-forming toxin[54,55], upon the addition of detergent on the timescale of seconds. To investigate the dynamics with single-molecule FRET, variants with two cysteine residues (BdpA: Y14C, P57C; ClyA: Q56C, E252C) were prepared and labeled with Alexa Fluor 488 and Alexa Fluor 594 as the FRET donor and acceptor dyes, respectively[17]. Details concerning the single-molecule instrumentation, data processing and the generation of corrected transfer efficiency histograms are described in refs. 12,26,29,50,56.

In the first mixing experiment, folded BdpA (100 pM) in 20 mM sodium acetate buffer (100 mM NaCl, 0.001% (vol/vol) Tween-20, 200 mM β-mercaptoethanol (pH 5)) was loaded in the center channel. The side channels contained the same buffer, but with no protein and the addition of 3.33 M guanidinium chloride as a denaturant. We obtained a mixing ratio of 1:10 and an average flow velocity of 1.0 μm ms^{-1} in the observation channel by applying the corresponding pressures (Step 55) to the three inlets (center: 16.8 kPa, side channels: 18.8 kPa). The final denaturant concentration of 3 M guanidinium chloride is close to the midpoint of the folding transition of BdpA at 22 °C. We recorded transfer efficiency histograms at 22 different positions along the observation channel (**Fig. 11**), corresponding to times after mixing in the range of 1 to 40 ms. Three representative transfer efficiency histograms are shown in **Figure 11d–f**. We expect the folding and unfolding kinetics of BdpA to occur on the milisecond timescale near the folding midpoint[53]. To resolve the folded and unfolded populations as separate peaks in the transfer efficiency histograms, we binned the photon bursts into time bins of 0.25-ms intervals and calculated the transfer efficiency for each bin. Three peaks are observed. The high transfer efficiency peak (E = 0.85) corresponds to the folded protein population, and the peak at E = 0.45 corresponds to the unfolded population. The third peak at E = 0 corresponds to proteins lacking an active acceptor dye. We fitted the histograms globally with a three-population model. Global fit parameters were the positions of the three peaks; the amplitudes and widths were fitted individually. For each histogram, the folded state population, p_{native}, was determined from the relative area under the native peak. The results are shown in **Fig. 11a** together with a single exponential fit of the form $p_{native}(t) = p_\infty + (1 - p_\infty)$ $\exp(-k(t - t_0))$. The fit decays to a final value $p_\infty = 0.39 \pm 0.02$. This value corresponds well to the expected value of $p_{eq} = 0.41$ measured for freely diffusing BdpA in an equilibrium experiment under identical buffer conditions. The rate constant is found to be $k = (0.54 \pm 0.07) ms^{-1}$, which is in excellent agreement with 0.56 ms^{-1} obtained from the equilibrium measurement using recurrence analysis[17]. The resulting value of time t_0 at which p_{native} extrapolates to 1 is 1.05 ± 0.30 ms before the time of the first measured point at position 28.75 μm. This result is in good agreement with the value from the corresponding position-to-time conversion (**Table 2**), which yields 1.03 ms for this position. Positions even closer to the mixing neck (<28.75 μm) correspond to smaller dead times, but the number of photons per fluorescence burst decreases strongly due to the steep increase in flow velocity (**Fig. 11c**) and due to the compromised fluorescence collection efficiency in the tapered part of the microfluidic channel[38].

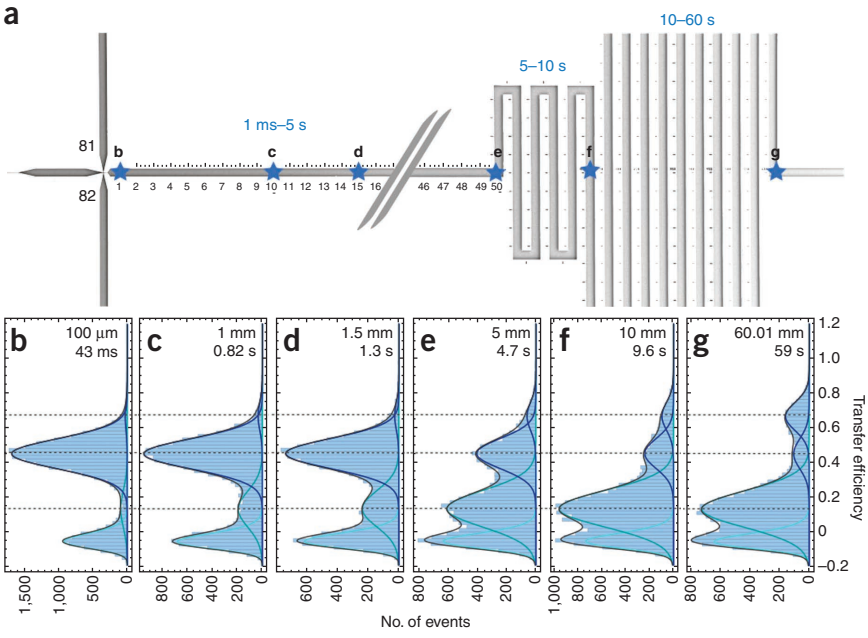

Figure 12 | Kinetic measurement of the conformational change of ClyA upon mixing with DDM. (**a**) Illustration of channel structures arranged from electron microscopy images of the mixing region and the observation channel. A section of 5 mm of straight observation channel (middle section omitted in the figure) is followed by two sets of serpentine channels; the first set adds 1 mm and the second set 5 mm per turn, respectively. (**a**–**g**) Blue stars in **a** indicate the positions where representative transfer efficiency histograms were recorded (**b**–**g**). The positions and the corresponding mean times after mixing are indicated. The histograms were fitted globally to a model with four populations (solid lines) with peak positions and widths as global fit parameters. Dashed lines indicate mean transfer efficiencies of the subpopulations.

In the second experiment, we loaded the center inlet with a buffer (20 mM potassium phosphate, 150 mM NaCl, 0.001% (vol/vol) Tween-20 (pH 7.4)) containing 1.6 nM of the monomeric form of the pore-forming toxin ClyA. The side inlets contained the same buffer with the addition of 0.1% of the detergent n-dodecyl-β-D-maltopyranoside (DDM), which induces large structural changes in the conformation of the protein[54,55]. The applied pressures were 16.1 kPa and 17.0 kPa at the center and side channels, respectively, to obtain a mixing ratio of 1:10 and an average flow velocity of 1.0 µm ms^{-1} in the observation channel. To prevent adhesion of ClyA to the channel walls, it was crucial to apply the passivation Steps 49–52. We recorded transfer efficiency histograms (for 20–30 min each) at different positions along the observation channel (**Fig. 12**), corresponding to different times after mixing (**Fig. 12a**). In this case, changes in at least three subpopulations are observed on a timescale between 100 ms and tens of seconds. At short times after mixing (**Fig. 12b**), a peak centered at E = 0.45 is observed, corresponding to the protein in its initial conformation, and a peak corresponding to molecules lacking an active acceptor at $E \approx 0$. In the following histograms, two additional peaks are observed. We attribute the peak at E = 0.13 to a transiently populated, more expanded conformation. At longer times (**Fig. 12e**,**f**), the final conformation (third peak at E = 0.66) becomes increasingly populated. Histograms recorded at ~15 min after (manual) mixing show only this final peak.

In summary, these examples illustrate the range of timescales accessible with the microfluidic mixer, from 1 ms to the minute range. For longer times, single-molecule measurements can be obtained from manual mixing experiments and sliding window analysis[54,55]. The resulting kinetics can then be combined in a global analysis, and a wide range of timescales becomes available for probing non-equilibrium single-molecule kinetics. Of course, data analysis is not limited to the accumulation of transfer efficiency histograms, as shown here for simplicity, but the entire spectrum of advanced analysis methods[26,49] can be applied to the data recorded, including fluorescence lifetimes, anisotropies, photon-counting histograms and correlation analysis. We thus anticipate that this microfluidic mixing device will be useful for many applications in which single-molecule spectroscopy is a suitable way of resolving heterogeneity and complex mechanisms in biomolecular reactions.

Note: Supplementary information is available in the online version of the paper.

ACKNOWLEDGMENTS We thank E. Lipman for many helpful suggestions and discussions that have led to the routine application of the microfluidic mixer to biomolecular dynamics. We thank S. Radford for labeled BdpA and R. Glockshuber and D. Roderer for discussion and for an expression plasmid for ClyA. We thank R. Kellner for help with photography and video recording, A. Schmid for technical support, A. Soranno for help with data analysis and A. Hoffmann for help in the initial stages of the project. We thank all users of the device in the group for their feedback and suggestions. Electron microscopy was performed with support of the Center for Microscopy and Image Analysis, University of Zurich. This work was supported by the Swiss National Science Foundation, the Swiss National Center of Competence in Research (NCCR) for Structural Biology and a Starting Grant of the European Research Council (to B.S.).

AUTHOR CONTRIBUTIONS B.W., D.N. and B.S. designed the research and wrote the manuscript with the help of the other authors. B.W. constructed the instrumentation and mixing device, performed the microfabrication and experiments, and established the practical procedures. B.W. and D.N. performed data analysis and finite element calculations. B.W., S.B., J.C. and H.H. performed the experiments with protein samples, and S.B. and D.N. contributed to the temperature-control calibration. S.W. contributed to the design of the machined parts. S.H.P. established large parts of the practical procedures and helped with the design and handling of the device.

COMPETING FINANCIAL INTERESTS The authors declare no competing financial interests.

1. Selvin, P.R. & Ha, T. *Single-Molecule Techniques: A Laboratory Manual* (Cold Spring Harbor Laboratory Press, 2008).

2. Dunkle, J.A. & Cate, J.H.D. Ribosome structure and dynamics during translocation and termination. *Annual Review of Biophysics* **39**, 227–244 (2010).
3. Marshall, R.A., Aitken, C.E., Dorywalska, M. & Puglisi, J.D. Translation at the single-molecule level. *Annu. Rev. Biochem.* **77**, 177–203 (2008).
4. Greenleaf, W.J., Woodside, M.T. & Block, S.M. High-resolution, single-molecule measurements of biomolecular motion. *Annu. Rev. Biophys. Biomol. Struct.* **36**, 171–190 (2007).
5. Kapanidis, A.N. & Strick, T. Biology, one molecule at a time. *Trends Biochem. Sci.* **34**, 234–243 (2009).
6. Ha, T., Kozlov, A.G. & Lohman, T.M. Single-molecule views of protein movement on single-stranded DNA. *Annu. Rev. Biophys.* **41**, 295–319 (2012).
7. Smiley, R.D. & Hammes, G.G. Single-molecule studies of enzyme mechanisms. *Chem. Rev.* **106**, 3080–3094 (2006).
8. Dittrich, P.S., Muller, B. & Schwille, P. Studying reaction kinetics by simultaneous FRET and cross-correlation analysis in a miniaturized continuous-flow reactor. *Phys. Chem. Chem. Phys.* **6**, 4416–4420 (2004).
9. Zhuang, X.W. Single-molecule RNA science. in *Annu. Rev. Biophys. Biomol. Struct.* **34**, 399–414 (2005).
10. Schuler, B. & Hofmann, H. Single-molecule spectroscopy of protein folding dynamics-expanding scope and timescales. *Curr. Opin. Struct. Biol.* **23**, 36–47 (2013).
11. Nettels, D., Gopich, I.V., Hoffmann, A. & Schuler, B. Ultrafast dynamics of protein collapse from single-molecule photon statistics. *Proc. Natl. Acad. Sci. USA* **104**, 2655–2660 (2007).
12. Soranno, A. *et al*. Quantifying internal friction in unfolded and intrinsically disordered proteins with single-molecule spectroscopy. *Proc. Natl. Acad. Sci. USA* **109**, 17800–17806 (2012).
13. Neuweiler, H., Johnson, C.M. & Fersht, A.R. Direct observation of ultrafast folding and denatured state dynamics in single protein molecules. *Proc. Natl. Acad. Sci. USA* **106**, 18569–74 (2009).
14. Sherman, E. & Haran, G. Fluorescence correlation spectroscopy of fast chain dynamics within denatured protein L. *Chemphyschem.* **12**, 696–703 (2011).
15. Chung, H.S., Cellmer, T., Louis, J.M. & Eaton, W.A. Measuring ultrafast protein folding rates from photon-by-photon analysis of single-molecule fluorescence trajectories. *Chem. Phys.* http://dx.doi.org/10.1016/j.chemphys.2012.08.005 (14 August 2012).
16. Schuler, B., Lipman, E.A. & Eaton, W.A. Probing the free-energy surface for protein folding with single-molecule fluorescence spectroscopy. *Nature* **419**, 743–747 (2002).
17. Hoffmann, A. *et al*. Quantifying heterogeneity and conformational dynamics from single-molecule FRET of diffusing molecules: recurrence analysis of single particles (RASP). *Phys. Chem. Chem. Phys.* **13**, 1857–1871 (2011).
18. Chung, H.S. *et al*. Extracting rate coefficients from single-molecule photon trajectories and FRET efficiency histograms for a fast-folding protein. *J. Phys. Chem. A* **115**, 3642–3656 (2011).
19. Gopich, I.V. & Szabo, A. FRET efficiency distributions of multistate single molecules. *J. Phys. Chem. B* **114**, 15221–15226 (2010).
20. Chung, H.S., Louis, J.M. & Eaton, W.A. Experimental determination of upper bound for transition path times in protein folding from single-molecule photon-by-photon trajectories. *Proc. Natl. Acad. Sci. USA* **106**, 11837–11844 (2009).
21. Chung, H.S., McHale, K., Louis, J.M. & Eaton, W.A. Single-molecule fluorescence experiments determine protein folding transition path times. *Science* **335**, 981–984 (2012).
22. Rhoades, E., Gussakovsky, E. & Haran, G. Watching proteins fold one molecule at a time. *Proc. Natl. Acad. Sci. USA* **100**, 3197–3202 (2003).
23. Rhoades, E., Cohen, M., Schuler, B. & Haran, G. Two-state folding observed in individual protein molecules. *J. Am. Chem. Soc.* **126**, 14686–14687 (2004).
24. Pirchi, M. *et al*. Single-molecule fluorescence spectroscopy maps the folding landscape of a large protein. *Nat. Commun.* **2**, 493 (2011).
25. Kuzmenkina, E.V., Heyes, C.D. & Nienhaus, G.U. Single-molecule Förster resonance energy transfer study of protein dynamics under denaturing conditions. *Proc. Natl. Acad. Sci. USA* **102**, 15471–15476 (2005).
26. Hofmann, H. *et al*. Single-molecule spectroscopy of protein folding in a chaperonin cage. *Proc. Natl. Acad. Sci. USA* **107**, 11793–11798 (2010).
27. Gambin, Y. *et al*. Visualizing a one-way protein encounter complex by ultrafast single-molecule mixing. *Nat. Methods* **8**, 239–241 (2011).
28. Lipman, E.A., Schuler, B., Bakajin, O. & Eaton, W.A. Single-molecule measurement of protein folding kinetics. *Science* **301**, 1233–1235 (2003).
29. Borgia, A. *et al*. Localizing internal friction along the reaction coordinate of protein folding by combining ensemble and single-molecule fluorescence spectroscopy. *Nat. Commun.* **2**, 1195 (2012).
30. Hamadani, K.M. & Weiss, S. Nonequilibrium single-molecule protein folding in a coaxial mixer. *Biophys. J.* **95**, 352–365 (2008).
31. Brody, J.P., Yager, P., Goldstein, R.E. & Austin, R.H. Biotechnology at low Reynolds numbers. *Biophys. J.* **71**, 3430–3441 (1996).
32. Knight, J.B., Vishwanath, A., Brody, J.P. & Austin, R.H. Hydrodynamic focusing on a silicon chip: mixing nanoliters in microseconds. *Phys. Rev. Lett.* **80**, 3863–3866 (1998).
33. Zimmerman, W.B.J. *Multiphysics Modeling with Finite Element Methods*, (World Scientific Publishing, 2006).
34. Hoffmann, A. *et al*. Mapping protein collapse with single-molecule fluorescence and kinetic synchrotron radiation circular dichroism spectroscopy. *Proc. Natl. Acad. Sci. USA* **104**, 105–110 (2007).
35. Kane, A.S. *et al*. Microfluidic mixers for the investigation of rapid protein folding kinetics using synchrotron radiation circular dichroism spectroscopy. *Anal. Chem.* **80**, 9534–9541 (2008).
36. Liu, K., Tian, Y., Burrows, S.M., Reif, R.D. & Pappas, D. Mapping vortex-like hydrodynamic flow in microfluidic networks using fluorescence correlation spectroscopy. *Analytica. Chimica. Acta.* **651**, 85–90 (2009).
37. Benninger, R.K. *et al*. Quantitative 3D mapping of fluidic temperatures within microchannel networks using fluorescence lifetime imaging. *Anal. Chem.* **78**, 2272–2278 (2006).
38. Pfeil, S.H., Wickersham, C.E., Hoffmann, A. & Lipman, E.A. A microfluidic mixing system for single-molecule measurements. *Rev. Sci. Instrum.* **80**, 055105 (2009).
39. Lemke, E.A. *et al*. Microfluidic device for single-molecule experiments with enhanced photostability. *J. Am. Chem. Soc.* **131**, 13610–13612 (2009).
40. Gambin, Y., Simonnet, C., VanDelinder, V., Deniz, A. & Groisman, A. Ultrafast microfluidic mixer with three-dimensional flow focusing for studies of biochemical kinetics. *Lab Chip* **10**, 598–609 (2010).
41. McDonald, J.C. & Whitesides, G.M. Poly(dimethylsiloxane) as a material for fabricating microfluidic devices. *Acc. Chem. Res.* **35**, 491–499 (2002).
42. Hofmann, H. *et al*. Polymer scaling laws of unfolded and intrinsically disordered proteins quantified with single-molecule spectroscopy. *Proc. Natl. Acad. Sci. USA* **109**, 16155–16160 (2012).
43. Arbour, T.J. & Enderlein, J. Application of dual-focus fluorescence correlation spectroscopy to microfluidic flow-velocity measurement. *Lab Chip* **10**, 1286–1292 (2010).
44. Roder, H., Maki, K. & Cheng, H. Early events in protein folding explored by rapid mixing methods. *Chem. Rev.* **106**, 1836–1861 (2006).
45. Cooksey, G.A., Plant, A.L. & Atencia, J. A vacuum manifold for rapid world-to-chip connectivity of complex PDMS microdevices. *Lab Chip* **9**, 1298–1300 (2009).
46. Nettels, D. *et al*. Single-molecule spectroscopy of the temperature-induced collapse of unfolded proteins. *Proc. Natl. Acad. Sci. USA* **106**, 20740–20745 (2009).
47. Kawahara, K. & Tanford, C. Viscosity and density of aqueous solutions of urea and guanidine hydrochloride. *J. Biol. Chem.* **241**, 3228–3232 (1966).
48. *CRC Handbook of Chemistry and Physics*, (CRC Press, 2013).
49. Sisamakis, E., Valeri, A., Kalinin, S., Rothwell, P.J. & Seidel, C.A.M. Accurate single-molecule FRET studies using multiparameter fluorescence detection. *Methods Enzymol.* **475**, 455–514 (2010).
50. Schuler, B. Application of single-molecule Förster resonance energy transfer to protein folding. *Methods Mol. Biol.* **350**, 115–138 (2007).
51. Gösch, M., Blom, H., Holm, J., Heino, T. & Rigler, R. Hydrodynamic flow profiling in microchannel structures by single-molecule fluorescence correlation spectroscopy. *Anal. Chem.* **72**, 3260–3265 (2000).
52. Dimitriadis, G. *et al*. Microsecond folding dynamics of the F13W G29A mutant of the B domain of staphylococcal protein A by laser-induced temperature jump. *Proc. Natl. Acad. Sci. USA* **101**, 3809–3814 (2004).
53. Arora, P., Oas, T.G. & Myers, J.K. Fast and faster: a designed variant of the B-domain of protein A folds in 3 microsec. *Protein Sci.* **13**, 847–853 (2004).
54. Mueller, M., Grauschopf, U., Maier, T., Glockshuber, R. & Ban, N. The structure of a cytolytic α-helical toxin pore reveals its assembly mechanism. *Nature* **459**, 726–730 (2009).
55. Eifler, N. *et al*. Cytotoxin ClyA from *Escherichia coli* assembles to a 13-meric pore independent of its redox-state. *EMBO J.* **25**, 2652–2661 (2006).
56. Schuler, B., Müller-Späth, S., Soranno, A. & Nettels, D. Application of confocal single-molecule FRET to intrinsically disordered proteins. *Methods Mol. Biol.* **896**, 21–45 (2012).
57. Dittrich, P.S. & Schwille, P. Spatial two-photon fluorescence cross-correlation spectroscopy for controlling molecular transport in microfluidic structures. *Anal. Chem.* **74**, 4472–4479 (2002).
58. Taylor, G. Conditions under which dispersion of a solute in a stream of solvent can be used to measure molecular diffusion. *Proc. Royal Soc. London A* **225**, 473–477 (1954).